Uptake Measurements of Acetic Acid on Ice and Nitric Acid–Doped Thin Ice Films over Upper Troposphere/Lower Stratosphere Temperatures

ARTICLE *in* THE JOURNAL OF PHYSICAL CHEMISTRY A · MARCH 2012

Impact Factor: 2.69 · DOI: 10.1021/jp205196t · Source: PubMed

4 AUTHORS, INCLUDING:

Manolis N Romanias
Ecole des Mines de Douai
25 PUBLICATIONS **99** CITATIONS
SEE PROFILE

Vassileios Papadimitriou
University of Crete
30 PUBLICATIONS **378** CITATIONS
SEE PROFILE

Panos Papagiannakopoulos
University of Crete
66 PUBLICATIONS **656** CITATIONS
SEE PROFILE

THE JOURNAL OF PHYSICAL CHEMISTRY A

Article

pubs.acs.org/JPCA

Uptake Measurements of Acetic Acid on Ice and Nitric Acid-Doped Thin Ice Films over Upper Troposphere/Lower Stratosphere Temperatures

Manolis N. Romanias, Antonia G. Zogka, Vassileios C. Papadimitriou, and Panos Papagiannakopoulos*

Laboratory of Photochemistry and Kinetics, Department of Chemistry, University of Crete, 71003 Heraklion, Crete, Greece

Supporting Information

ABSTRACT: The adsorption of gaseous acetic acid ($CH_3C(O)OH$) on thin ice films and on ice doped with nitric acid (1.96 and 7.69 wt %) was investigated over upper troposphere and lower stratosphere (UT/LS) temperatures (198−208 K), and at low gas concentrations. Experiments were performed in a Knudsen flow reactor coupled to a quadrupole mass spectrometer. The initial uptake coefficients, γ_0, on thin ice films or HNO_3-doped ice films were measured at low surface coverage. In all cases, γ_0 showed an inverse temperature dependence, and for pure thin ice films, it was given by the expression $\gamma_0(T) = (4.73 \pm 1.13) \times 10^{-17} \exp[(6496 \pm 1798)/T]$; the quoted errors are the 2σ precision of the linear fit, and the estimated systematic uncertainties are included in the pre-exponential factor. The inverse temperature dependence suggests that the adsorption process occurs via the formation of an intermediate precursor state. Uptakes were well represented by the Langmuir adsorption model, and the saturation surface coverage, N_{max}, on pure thin ice films was $(2.11 \pm 0.16) \times 10^{14}$ molecules cm^{-2}, independent of temperature in the range 198−206 K. Light nitration (1.96 and 7.69 wt %) of ice films resulted in more efficient $CH_3C(O)OH$ uptakes and larger N_{max} values that may be attributed to in-bulk diffusion or change in nature of the gas−ice surface interaction. Finally, it was estimated that the rate of adsorption of acetic acid on high-density cirrus clouds in the UT/LS is fast, and this is reflected in the short atmospheric lifetimes (2−8 min) of acetic acid; however, the extent of this uptake is minor resulting in at most a 5% removal of acetic acid in UT/LS cirrus clouds.

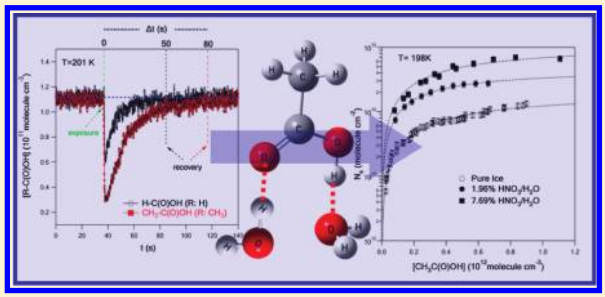

INTRODUCTION

Carboxylic acids are among the most abundant volatile organic compounds (VOC) in the atmosphere, with mixing ratios up to 792 ppt.[1,2] They are generated in the atmosphere via several homogeneous and heterogeneous photochemical processes or directly emitted via biogenic[3] and anthropogenic activities.[1] They are potent sources of HO_x radicals[4] in the troposphere and participate in the photochemical cycle of O_3.[5] Furthermore, carboxylic acids are quite soluble organic acids and appear as intermediate species during the oxidation process of several hydrocarbons in the atmosphere or in the aqueous phase.[6] However, less attention has been given to the heterogeneous reactions of carboxylic acids with ice surfaces, although such species are abundant in free troposphere and may play an important role in the chemistry of the upper troposphere.[7,8]

Moreover, nitric acid traces have been detected in several field measurement studies in the mid and upper troposphere, with mixing ratios in the range 0.1−2 ppb,[9] as well as in the low stratosphere, as stable crystalline nitric acid trihydrates (NAT).[10] Furthermore, nitric acid molecules are trapped in ice particles during their growth process at the existing low temperatures in the upper troposphere/low stratosphere (UT/LS),[10,11] resulting in HNO_3-doped ice particles or NAT formation. Therefore, it is critical to study the interaction of carboxylic acids with ice films doped with HNO_3.

The heterogeneous interaction of carboxylic acids with pure ice films at low temperatures has been investigated only by a few experimental studies.[12−16] In particular, the adsorption of acetic acid ($CH_3C(O)OH$) on ice surfaces has been studied mainly by the coated-wall laminar flow tube (CWLFT) technique[17−20] and several theoretical calculations.[21−23] However, there are no experimental data for the initial uptake coefficients, γ_0 (IUPAC terminology is adopted[24]), of $CH_3C(O)OH$ on pure ice films or on thin ice films doped with HNO_3, at low temperatures.

The aim of the present study was to investigate the uptake of $CH_3C(O)OH$ on pure and HNO_3-doped ice surfaces, at low temperatures relevant to the UT/LS. First, the initial uptake coefficients, γ_0, of $CH_3C(O)OH$ on thin pure ice films and ice doped with 1.96 and 7.69 wt % of HNO_3 were measured at low temperatures between 198 and 208 K, and low gas concentrations. Furthermore, the surface coverage, N_s, of $CH_3C(O)OH$ on thin pure and HNO_3-doped ice films were measured at low ice temperatures; the saturation surface coverage, N_{max}, and partition coefficients, K_{Lin}, were derived by employing the Langmuir adsorption model. Finally, the potential removal of

Received: June 2, 2011
Revised: February 7, 2012
Published: February 8, 2012

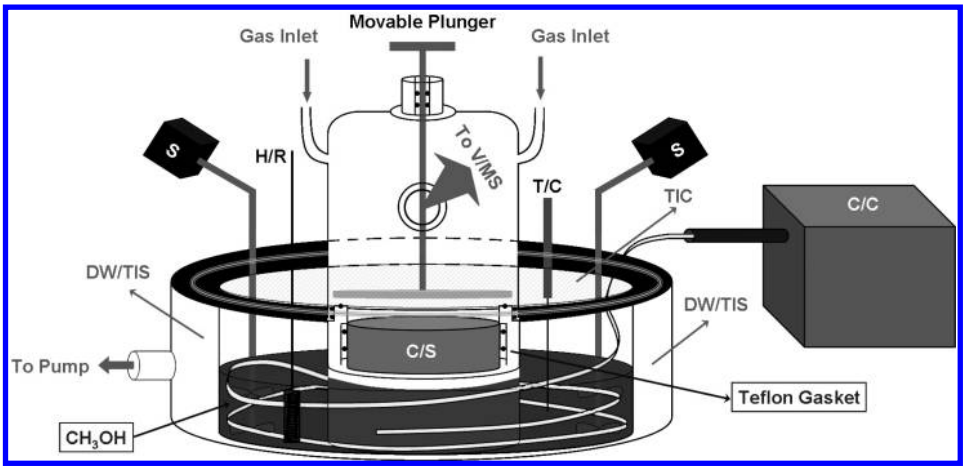

Figure 1. Overall schematic diagram of a Knudsen reactor in which the major components are presented: (a) $CH_3C(O)OH$ and H_2O vapor inlets, and the movable plunger in the upper part; (b) the external Teflon and the inner copper flanges (C/S) connected via Viton O-rings in the bottom part; and (c) the side outlet connecting the reactor with the quadrupole mass spectrometer chamber. The ice films are grown on the upper round part of the copper flange (C/S), while the bottom part is cooled by a methanol bath cryostated with a refrigerator unit. Abbreviations used in the figure: C/S, copper substrate; C/C, cooling circulating unit; S, electrical stirrer; V/MS, vacuum/mass spectrometry system; T/C: thermocouple; DW/TIS, double walled thermally isolated system; H/R, heating resistance; and TIC, thermal isolating cover.

Table 1. Characteristic Parameters of Knudsen Reactor

parameters	expression	value
total reactor volume (V_R)		535 cm^3
compartment volume (V_C)		13 cm^3
ice surface area (A_s)		12.56 cm^2
diameter of escape orifice (d)		2 and 5 mm
ice surface area/orifice surface area (A_s/A_h)		400 (d = 2 mm); 64 (d = 5 mm)
escape rate coefficient ($k_{esc,M}$)[a]	$k_{esc,M}$[b] = 0.164 $(T/m)^{1/2}$ (2 mm); $k_{esc,M}$[b] = 0.732 $(T/m)^{1/2}$ (5 mm)	0.38 s^{-1} (d = 2 mm); 1.69 s^{-1} (d = 5 mm)
gas concentration ([M])	[M] = F_M[c]/($k_{esc,M}V_R$)	(4.6–47) × 10^{10} cm^{-3}
frequency of collisions on ice surface (ω)	$\omega = u_M A_s/4V_R$	199 s^{-1}
number of collisions on ice surface		524 (d = 2 mm); 117 (d = 5 mm)
uptake coefficient (γ)	$\gamma = k_{upt}/\omega$	

[a]All experiments presented in Figures 2–6 have been carried out using 2 mm exit aperture, as well as the majority of the measurements presented herein, unless otherwise stated. [b]Derived from separate calibration experiments. [c]F_M is the molecular flow rate (in molecule s^{-1}).

$CH_3C(O)OH$ molecules from the atmosphere, via heterogeneous interaction with pure or HNO_3-doped ice particles in cirrus clouds at the UT/LS, was examined.

EXPERIMENTAL SECTION

The adsorption of $CH_3C(O)OH$ on thin ice films were determined by performing uptake experiments employing a continuous flow molecular system equipped with a Knudsen reactor (Kn) and a quadrupole mass spectrometer (QMS). The Kn/QMS technique has been used extensively in the past to measure absolute reaction rate coefficients of Cl atoms with volatile hydrocarbons in the gas phase,[25,26] and more recently to measure uptake coefficients and coverage of formic acid on thin ice films.[27] Therefore, only a brief description of the experimental setup will be presented herein. The experimental setup consisted of the gas preparation vacuum line, the Knudsen flow reactor, and the differentially pumped stainless steel high-vacuum chamber that includes a quadrupole mass spectrometer (Inficon, QMG 422) in the inner chamber. The molecular flows were modulated by a skimmer/tuning-fork chopper operating at 200 Hz. Subsequently, mass spectrometric (MS) signals were filtered and amplified with a lock-in amplifier (SR8300, DSP) and finally stored digitally in a computer for further analysis.

The Knudsen reactor was made out of glass, with a water-titrated total volume of 535 cm^3, equipped with three inlets on the top for introducing gas reactants, and one outlet on the side for effusing reactants and products (via a variable-diameter sliding exit aperture, d = 1–5 mm) to the differentially pumped system, as shown in Figure 1. The characteristic parameters of the Knudsen reactor are given in Table 1. The bottom part consisted of a round copper cylindrical disk (surface area, A_s = 12.56 cm^2) that was connected to the glass part with two O-ring Teflon flanges, upon which thin ice films were grown. Ice films were isolated or exposed to the molecular flow by sliding a Teflon plunger from the lower to upper position, respectively. The lower part of the copper disk was immersed in a pumped double wall methanol bath vessel, which was cooled via a refrigerator unit (Haake, EK90). The methanol bath temperature was controlled within ±1 K, via a thermostat (Shimaden, SR91, $\Delta T = \pm 0.1$ K) in conjunction with a heating resistance. The Knudsen reactor internal wall was coated with thin Teflon film (Du-Pont, FEP 121A), while the external wall

dx.doi.org/10.1021/jp205196t | J. Phys. Chem. A 2012, 116, 2198–2208

was heated at 323 K to maintain constant temperature and prevent condensation of water on the internal wall.

Thin ice films were prepared by flowing water vapors at a flow rate ~2.6 × 10^{17} molecule s^{-1} ([H_2O] ≈ 7.0 × 10^{14} molecules cm^{-3}) over the cold copper surface at 206 K for 20 min. The exact procedure has been described in detail previously.[27] The ice films' thickness was estimated to be 5−6 μm, and it was maintained by introducing a steady flow of water vapor in the reactor, during the uptake experiments. The water flow rate was adjusted in every experiment to compensate for ice evaporation, by verifying that water partial concentration (I_{18} mass signal) did not change by moving the plunger from the upper to lower position. These water flow rates at different temperature and pressure reactor conditions are given in Table 2. Pratte et al.[28] have studied the kinetics of condensation and evaporation for different types of ice surfaces and obtained the evaporation fluxes (J_{ev}, molecule s^{-1} cm^{-2}) of H_2O in the temperature range 130−210 K, by measuring the condensation rate constants (k_c, s^{-1}). The authors clearly indicate that J_{ev} values of the condensed ice film depend on the conditions employed during H_2O(g) deposition and ice surface formation processes (substrate temperature, H_2O flow rate, residence time, and steady-state concentration). Our J_{ev} values were estimated by using the expression $J_{ev} = F_{ev}/A_s = (k_c F_{ss})/(k_{esc,H2O} A_s)$,[28] where A_s is the ice surface area in cm^2 and F_{ss}, the ice evaporation compensating water flow rate. Adopting their k_c values,[28] our J_{ev} were systematically lower by a factor of ~4 compared to their values over the whole temperature range. Assuming that the k_c values used are valid under our experimental conditions, the observed discrepancy in J_{ev} can be probably attributed to the different experimental conditions employed during the ice film formation, namely, (a) the temperature and duration of ice film preparation (ΔT = 26 K and Δt = 10 min), (b) the gas phase H_2O concentration (10 times higher), and (c) H_2O residence time (different by a factor of ~4 or ~0.05). These differences in experimental conditions might affect the structure and smoothness of the ice surfaces and their reactivity, leading to substantially different physicochemical properties of the formed ice surfaces. Thus, the lower J_{ev} values obtained herein might indicate ice surfaces with fewer structural defects. It is worthy to note that a full evaluation of this discrepancy would require a systematic measurement of k_c and J_{ev} for ice surfaces prepared under different temperature conditions, which was beyond the scope of the present study.

Table 2. Initial Uptake Coefficient γ_0 Values for $CH_3C(O)OH$ Uptakes on Pure Ice Films and on Ice Films Doped with 1.96 and 7.69 wt % HNO_3 at Various Temperatures[a]

T (K)	[$CH_3C(O)OH$][b]	# expts	γ_0 (10^{-3})	F_{H2O}[c]
		Pure Ice		
201	0.46−2.88	6	4.7 ± 0.3	1.18 ± 0.03
203	0.52−3.36	4	4.1 ± 0.2	1.65 ± 0.04
206	0.84−3.73	6	2.5 ± 0.2	2.44 ± 0.06
208	0.81−4.70	8	1.6 ± 0.2	3.19 ± 0.09
		Ice Doped with 1.96 wt % HNO_3		
198	0.84−5.09	8	4.8 ± 1.0	0.80 ± 0.01
201	1.25−3.03	3	3.5 ± 0.4	1.14 ± 0.02
203	0.78−4.92	7	2.9 ± 0.4	1.62 ± 0.03
		Ice Doped with 7.69 wt % HNO_3		
198	1.36−6.43	12	7.7 ± 0.5	0.77 ± 0.01
201	0.84−4.08	5	5.0 ± 0.7	1.10 ± 0.02
203	0.72−5.16	6	3.6 ± 0.4	1.51 ± 0.03
206	0.87−4.39	5	2.4 ± 0.3	2.33 ± 0.05

[a]The quoted uncertainties represent the precision and are given at 95% level of confidence. The H_2O flow rates (molecule s^{-1}) used to balance the ice vapor pressure are given in the last column. [b][$CH_3C(O)OH$] in 10^{11} molecules cm^{-3}. [c]F_{H2O} in 10^{16} molecule s^{-1}.

The ice temperature was determined within ±1 K by measuring the steady-state H_2O concentration inside the reactor, by using the expression [H_2O] = $I_{18}/(a_{H2O} k_{esc,H2O} V_R)$, where I_{18} was the MS signal intensity of H_2O, $k_{esc,H2O}$ was the escape rate coefficient in s^{-1}, V_R was the titrated reactor volume in cm^3, and a_{H2O} was the H_2O MS signal-flow calibration factor in s $molecule^{-1}$ that was determined in separate flow calibration experiments (Supporting Information, Figure S1). HNO_3-doped ice films were prepared by flowing concurrently H_2O and HNO_3/He mixtures over the copper surface at 206 K for 30−60 min via separate inlets; more details are given previously.[27] H_2O and HNO_3 steady-state concentrations in the Knudsen reactor were in the range (0.5−2) × 10^{14} molecules cm^{-3} and (1−10) × 10^{13} molecules cm^{-3}, respectively. According to the phase diagram of the HNO_3/H_2O binary system, mixtures of 1.96−7.69 wt %, at temperatures below 230 K, are always in the solid phase domain.[29]

The morphology and structure of pure or HNO_3-doped ice films produced by vapor deposition of H_2O or H_2O/HNO_3 at low temperatures (180−200 K) and pressures (~0.05 Torr) have been studied in the past using ESEM[30−32] and FTIR[12,33,34] techniques. According to these studies, the pure ice films formed at temperatures lower than 180 K consist of ice particles with hexagonal structure and average size of ~5 μm, while the corresponding ice films formed at higher temperatures, up to 215 K, still retain their hexagonal structure.[30−32] Moreover, it has been observed that lightly HNO_3-doped ice films grown at 200 K consist of a supercooled HNO_3/H_2O solution that converts to crystalline nitric acid trihydrate (NAT, $HNO_3 \cdot 3H_2O$) under slightly undersaturated conditions of H_2O.[12,33] In the present work, ice films were prepared using similar methodology and low temperature−pressure conditions; therefore it is most likely to have analogous morphology and structure.

It is also known that $CH_3C(O)OH$ undergoes dimerization under certain pressure and temperature conditions.[35,36] In the Knudsen reactor, the mean thermal energy of $CH_3C(O)OH$ molecules, prior to adsorption, was determined by the wall temperature (323 K), in distinction to the low wall temperatures of the CWLFT reactor. $CH_3C(O)OH$ monomers and dimers are in equilibrium within 20 ms,[18] which is much faster than their residence time in a Knudsen reactor (~ 2.6 s). It is estimated that the mole fraction of $CH_3C(O)OH$ dimers in our experiments was always less than 0.1% since [$CH_3C(O)OH$] < 1.2 × 10^{12} molecules cm^{-3}, and therefore, dimers have an insignificant contribution. In addition, surface coverage was determined using either MS signals at m/z = 45 or m/z = 60, and the obtained values were identical, indicating that both MS signals originate from a single species, $CH_3C(O)OH$ monomer.

Another issue of concern was the probable dissociation and ionization of $CH_3C(O)OH$ molecules upon striking the ice surface since their thermal energy at room temperature is ~4 kJ mol^{-1}. Although such processes have been predicted theoretically[21] and partly observed at similar low temperature and pressure conditions,[37] it was investigated by performing separate uptake experiments of $CH_3C(O)OH$ and HCl on D_2O

dx.doi.org/10.1021/jp205196t | J. Phys. Chem. A 2012, 116, 2198−2208

ice surfaces. Limited dissociation of $CH_3C(O)OH$ in the ice surface will produce acetate that may either diffuse into the ice bulk or be neutralized by a deuteron and further desorbed in the gas phase as deuterated acetic acid. The interaction of HCl (strong acid) on the ice surface resulted in the formation of DCl product, indicating H/D exchange on and/or inside the ice surface. On the contrary, the interaction of $CH_3C(O)OH$ (weak acid) with D_2O ice surface did not produce any deuterated acetic acids, within detection limits, excluding any significant degree of dissociation and/or ionization. Furthermore, uptake signals of $CH_3C(O)OH$ on pure and 1.96 wt % HNO_3-doped ice films return to their initial steady-state value within ~100 s (Figure 2 and Supporting Information, Figure S2),

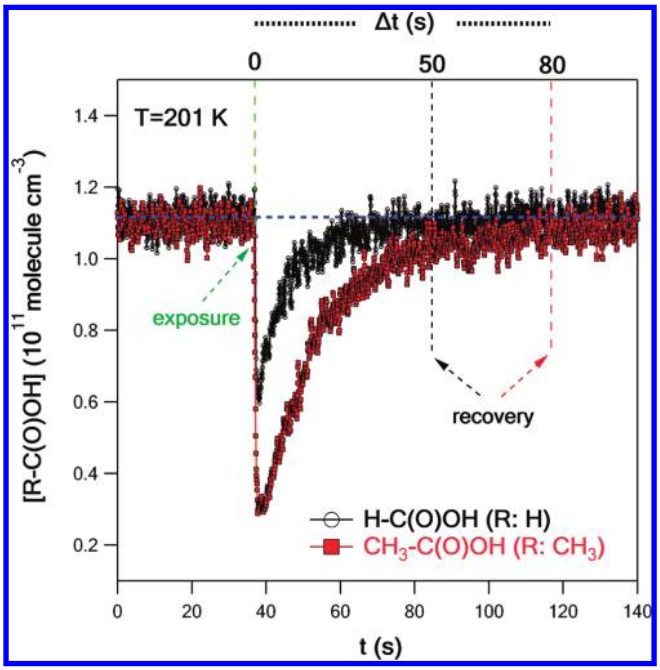

Figure 2. Typical profile of uptake signals for HC(O)OH and $CH_3C(O)OH$ (~1×10^{11} molecules cm^{-3}) on pure ice films at 201 K. The surface coverage (N_s) on ice films (molecules cm^{-2}) were determined by integrating the area under these uptake profiles. The exposure time of $CH_3C(O)OH$ on the ice surface and the recovery time of uptake signal are depicted with vertical dashed lines.

suggesting insignificant in-bulk diffusion. However, uptake signals on 7.69 wt % HNO_3-doped ice films return to their 2/3 value within ~100 s and saturate at ~80% at later times (Supporting Information, Figure S2), indicating possible divergence from the Langmuir adsorption model and in-bulk diffusion or change in nature of heterogeneous interaction. Finally, the experimental data for surface coverage on pure and HNO_3-doped ice films did not obey the dissociative adsorption kinetics[38] but followed satisfactorily the Langmuir adsorption model, indicating no appreciable degree of dissociation.

Uptake Kinetic Measurements. In a Knudsen reactor, the steady-state concentration of gaseous molecules is determined by using the following expression:

$$[M] = F_M/(k_{esc,M}V_R) = I_M/(a_M V_R k_{esc,M}) \quad (1)$$

where I_M is the MS signal intensity, a_M is the MS signal-flow calibration factor (s $molecule^{-1}$), V_R is the Knudsen reactor volume (cm^3), $k_{esc,M}$ is the escape rate coefficient (s^{-1}) given in Table 1, and F_M is the molecular flow rate (molecule s^{-1}). Molecular flows were created by flowing molecules from a titrated buffer volume (985 cm^3) into the Knudsen reactor, via a 9 cm long thin-capillary tube (0.6 mm internal diameter). Molecular flow rates, F_M, were determined by separate calibration experiments, in which the pressure drop at the high-pressure end of the capillary was recorded as a function of time, using pressure transducers with accuracy <1%; more details are presented elsewhere.[26] MS signal-flow calibration factors a_M were determined daily by plotting I_M versus F_M, over the actual experimental pressure range, with error limits less than 3% at 95% level of confidence (Supporting Information, Figure S3). $CH_3C(O)OH$ was followed by recording both parent and fragment ion peaks at m/z 60 and 45, respectively, at electron energy 70 eV, with 2σ precision of ~1%.

A typical profile of uptake signals for $CH_3C(O)OH$ on a thin ice film at 201 K is displayed in Figure 2. The initial fast drop of the uptake signal (~2 s) provides the initial uptake coefficients γ_0, while the enclosed area of the uptake signals (~100 s) over the geometric ice-surface (A_s) provides the surface coverage N_s (molecules cm^{-2}). The latter corresponds to the total number of $CH_3C(O)OH$ molecules adsorbed on the ice surface, assuming that no diffusion or chemical processes occur in the ice bulk. Note that MS signal intensities (I_M) were converted to molecular flow rates (F_M) using eq 1. It is worth mentioning that the above assumptions are reasonable for pure and 1.96 wt % HNO_3-doped ice films since the Langmuir-isotherm fits to the experimental data were excellent, and uptake signals were returning to their initial steady-state value within ~100 s. Even in the case of 7.69 wt % HNO_3-doped ice films, uptake signals were leveled-off at later times (t > 100 s) reaching at least to 80% of the initial steady-state value (t = 0), and N_s values satisfactorily followed the Langmuir adsorption model.

In the Knudsen reactor, under molecular flow conditions, the experimental initial uptake coefficient, γ_0, is given by the following expression:

$$\gamma_0 = \frac{k_{upt}}{\omega} = \frac{4V_R k_{esc,M}}{u_M A_s}\frac{(F_{0,M} - F_{r,M})}{F_{r,M}} = \frac{4V_R k_{esc,M}}{u_M A_s}\frac{(I_{0,M} - I_{r,M})}{I_{r,M}} \quad (2)$$

where $\omega = u_M A_s/4V_R$ is the collision frequency of gas molecules on the ice surface (s^{-1}), $u_M = 1.46 \times 10^4 (T/m)^{1/2}$ is the mean molecular velocity (cm s^{-1}), with T and m the temperature (K) and molar mass (g mol^{-1}), respectively. A_s is the ice surface area (cm^2), and V_R is the reactor volume (cm^3). k_{upt} is the uptake rate coefficient (s^{-1}) with $k_{upt} = k_{esc,M}(F_{0,M} - F_{r,M})/F_{r,M}$, where $k_{esc,M}$ is the escape rate coefficient (s^{-1}). $F_{r,M}$ and $F_{0,M}$ are the molecular flow rates (molecule s^{-1}) at the maximum level (~2 s) with and without gas exposure to the ice surface, respectively, which are correlated to MS signal intensities ($I_{r,M}$ and $I_{0,M}$) via the expression $I_M = a_M F_M$. All characteristic parameters for the Knudsen reactor are given in Table 1.

More precisely, γ_0 was determined by recording the MS signal intensity at the two extreme plunger positions: (a) plunger at the down position isolating the ice surface from the gas molecular flow, allowing only the competition between $CH_3C(O)OH$ inflow and escape from the reactor, and recording the steady-state mass spectral intensity as $I_{0,M}$, and (b) plunger at the upper position exposing the ice surface to the

dx.doi.org/10.1021/jp205196t | J. Phys. Chem. A 2012, 116, 2198–2208

molecular flow, allowing the adsorption process to compete with the flow-in and flow-out from the reactor, and by recording the MS signal at the lowest level of the uptake profile (~2 s), corresponding to $I_{r,M}$. In particular, $I_{r,M}$ was determined by averaging the values at the lowest level with ±2% variance (~15 data points) that corresponds to the maximum MS signal uncertainty. Additional experiments were performed with molecular flows of $CH_3C(O)OH$ in the absence of ice surfaces and by sliding the plunger from the upper to the lower position, in order to assess the impact of reactor's volume change (~2%) to MS signal intensity. There was no measurable variation in the MS signals (<1%), which implies no such interference in our measurements.

Another cause of concern was the possible dependence of γ_0 on the escape rate coefficient $k_{esc,CH3C(O)OH}$. Therefore, initial uptake measurements were performed with two escape orifices, d = 2 and 5 mm, under identical initial $CH_3C(O)OH$ steady-state concentrations. It was found that γ_0 values for both escape rate coefficients 0.38 (d = 2 mm) and 1.69 (d = 5 mm) s^{-1} at 201 K were equal, $(4.7 \pm 0.3) \times 10^{-3}$, which verifies the validity of eq 2. This was also true in previous uptake experiments with formic acid on ice.[27]

Materials. The chemicals/gases used in this study were commercially available with stated purity or synthesized. $CH_3C(O)OH$ (Sigma-Aldrich, 96%) was purified by fractional distillation and repeated freeze−pump−thaw cycles and was diluted in He (Linde, 99.7%) to 0.78, 1.10, 2.83 and 4.65% $CH_3C(O)OH$/He mixtures. Nitric acid was synthesized via the reaction of sulfuric acid with potassium nitrate and was further cryo-trapped at 77 K. Subsequently, 7.4 and 8.5% HNO_3/He mixtures were manometrically prepared and were stored in a dark glass bulb, to avoid decomposition to NO_2. Their purity was often verified by performing mass spectrometry and FTIR spectroscopy analysis. At first, the mass fragmentation of HNO_3, NO_2, and NO was quantified in our system (at 70 eV ion source electron voltage), by separate flow experiments. It was determined that both HNO_3 and NO_2 contribute to I_{46} and I_{30} mass peaks with ratios $I_{46}/I_{30} \approx 1.7$ and ~0.3, respectively, while NO contributes only to I_{30}. Therefore, the presence of NO and/or NO_2 impurities in HNO_3 mixtures will result in lower I_{46}/I_{30} ratios. In our uptake experiments of $CH_3C(O)OH$ on HNO_3-doped ice films, the I_{46}/I_{30} ratio was always monitored continuously and was constant at ~1.7, indicating no observable degradation of HNO_3. Furthermore, the IR spectrum of HNO_3 mixtures was taken, while the IR absorption cross-sections of purified HNO_3, NO_2, and NO were determined previously using the Beer−Lambert law. The FTIR analysis confirmed that the impurity of NO_2 and NO in HNO_3/He mixtures were always less than 1%. It is worth mentioning that uptakes of NO_2 and NO on ice films were also measured at 206 K, and their values were negligible compared to those of HNO_3. Therefore, even if low levels (<1%) of NO and NO_2 are present in HNO_3 mixtures, they will result in an insignificant effect on our uptake measurements. Nanopure H_2O was used for the preparation of the ice films that was previously degassed by several freezing/melting cycles. Finally, total pressure, P, in the Knudsen reactor for d = 2 and 5 mm apertures was always less than 9 and 3 mTorr, respectively, corresponding to dP = 1.8 and 1.5 (d in cm and P in mTorr), ensuring molecular flow conditions (dP < 5.09).

Error Analysis. In this section, we consider possible systematic contributions to the absolute uncertainty of $\gamma_0(T)$ and N_s. They mainly include systematic uncertainties in the determination of $CH_3C(O)OH$ concentration and experimental parameters such as ice temperature, reactor temperature and volume, and pressure in molecular flows. MS signals were measured with high precision, and the 2σ was always better than 2%. Note that all error limits given herein are reported at 95% level of confidence. Uncertainties in water-titrated reactor volume, escape rate coefficient, temperature, and pressure measurements were 1%, 2%, 1%, and 1%, respectively. The larger source of systematic errors in concentration determination (using eq 1) is attributed to the molecular flow rates that are reflected to the MS signal-flow calibration factors, a_M. The uncertainty in a_M determination was ~3%,[26] while the 2σ precision was very high. Typical calibration plots (I_M vs F_M) for H_2O and $CH_3C(O)OH$ are presented in Supporting Information Figures S1 and S3, respectively. Pressure, reactor's volume, and temperature errors contribute to less than 1% separately to the overall estimated uncertainties. Moreover, the uncertainty in escape rate coefficients ($k_{esc,M}$) is ~2%. Thus, the overall systematic uncertainty in concentration determination was ~4%. Another source of systematic uncertainties in N_s and γ_0 measurements is related to the ice temperature determination. Both methods employed for ice temperature measurement, as described below, agreed within 3%, and the temperature variation within an experiment was less than 1%. Ice surface area and gas-mixture dilution, by moving-up the plunger, systematic errors contribute to less than 2% to the overall uncertainty. $CH_3C(O)OH$ in-bulk diffusion had a variable effect in systematic uncertainty depending on the level of HNO_3 doping, and the ice temperature. The estimated contribution for pure ice surfaces was less than 2%, while for highly HNO_3-doped ice surfaces, it was estimated to be ~7% at the lowest temperature, where the largest effect was observed. γ_0 measurements are expected to be less sensitive to in-bulk diffusion since the whole process is completed within the two first seconds, compared to N_s that is determined within ~100 s time frame. However, a safe constant 7% error limit was included in the estimated systematic uncertainty for both γ_0 and N_s determinations. Finally, it should be noticed that the random errors in γ_0 uncertainty estimation had a larger effect compared to N_s since in the first case the absolute variation in mass spectral intensity was measured, while in N_s determination, the integral of the enclosed uptake profile ($F_M(t)$) is required. Therefore, the estimated systematic uncertainties (accuracy) were estimated to be 9%, while the overall uncertainty, including the 2σ precision (repeatability and reproducibility) of the measurements, is given by the expression (uncertainty)^2 = (2σ precision)^2 + (systematic errors)^2. The upper limit for N_s uncertainty was ~10%, while the γ_0 overall error limits were estimated to be up to 12% and 21% for pure ice and HNO_3-doped surfaces, respectively.

RESULTS AND DISCUSSION

Initial Uptake Coefficients of $CH_3C(O)OH$ on Ice. A typical profile of uptake signals for $CH_3C(O)OH$ on thin ice films at 201 K is shown in Figure 2. Similar profiles have been obtained previously in this lab for HC(O)OH uptake signals at identical conditions.[27] The initial uptake coefficient, γ_0, of $CH_3C(O)OH$ on thin ice films was determined as a function of $CH_3C(O)OH$ concentration in the range $(0.5-4.7) \times 10^{11}$ molecules cm^{-3}, at various temperatures, 201−208 K, and they are presented in Table 2. To our knowledge, this is the first experimental study that γ_0 values for $CH_3C(O)OH$ on pure ice surfaces were measured. Thus, our γ_0 values can only be

Table 3. Surface Coverage, N_s, Values of $CH_3C(O)OH$ on 1.96 and 7.69 wt % HNO_3-Doped Ice Surfaces As a Function of $CH_3C(O)OH$ Concentration at Different Ice Temperatures

1.96 wt % (HNO_3/H_2O)[a]		
$[CH_3C(O)OH]$ (10^{11} molecules cm^{-3})	N_s (10^{14} molecules cm^{-2})	$[CH_3C(O)OH]/N_s$ (10^{-4} cm^{-1})
T = 198 K		
0.84	0.74	11.4
1.42	1.19	11.9
1.88	1.43	13.2
2.47	1.74	14.2
3.04	2.00	15.2
3.77	2.29	16.5
4.44	2.52	17.6
5.10	2.66	19.2
5.84	2.72	21.5
6.61	2.76	24.0
T = 201 K		
1.25	0.61	20.5
2.14	0.84	25.5
3.03	1.02	29.71
3.95	1.14	34.6
5.30	1.40	37.9
6.65	1.52	43.8
7.58	1.66	45.7
T = 203 K		
2.06	0.68	30.3
2.72	0.84	32.4
3.57	1.10	32.4
4.62	1.16	39.8
5.64	1.34	42.1
7.69 wt % (HNO_3/H_2O)[a]		
$[CH_3C(O)OH]$ (10^{11} molecules cm^{-3})	N_s (10^{14} molecules cm^{-2})	$[CH_3C(O)OH]/N_s$ (10^{-4} cm^{-1})
T = 198 K		
0.80	1.04	7.69
1.36	1.62	8.40
1.66	1.85	8.97
2.42	2.84	8.52

7.69 wt % (HNO_3/H_2O)[a]		
$[CH_3C(O)OH]$ (10^{11} molecules cm^{-3})	N_s (10^{14} molecules cm^{-2})	$[CH_3C(O)OH]/N_s$ (10^{-4} cm^{-1})
T = 198 K		
2.74	2.98	9.19
3.29	3.82	8.61
3.57	3.54	10.1
4.43	5.10	8.69
4.62	4.66	9.91
5.72	5.56	10.3
6.94	6.47	10.7
8.32	6.93	12.0
11.1	6.63	16.7
T = 201 K		
0.84	0.83	10.1
1.58	1.39	11.4
2.45	1.95	12.6
3.10	2.19	14.2
4.08	2.55	16.0
5.40	2.97	18.2
6.77	3.39	20.0
7.91	3.58	22.1
8.98	3.67	24.5
10.2	3.76	27.0
11.2	3.79	29.5
T = 206 K		
0.87	0.34	25.6
1.75	0.64	27.3
2.55	0.85	30.0
3.52	0.99	35.6
4.39	1.11	39.6
5.41	1.22	44.3
6.70	1.35	49.6
7.84	1.44	54.4
9.09	1.50	60.6
5.16	1.20	43.0

[a]Percentage corresponds to the mixing ratio of the flowing mixture used to form the ice surface.

compared to those reported for HC(O)OH and other atmospheric trace gases, at similar ice surface temperature range. γ_0 values presented herein are lower compared to the corresponding ones determined for OH, HCl, HNO_3, CH_3OH, N_2O_5, and $CH_3C(O)CH_3$ gases, similar to those for HONO, and higher or much higher than those for HC(O)OH, NO_3, NO_x, and O_3.[24]

The initial uptake coefficient, γ_0, was determined by the initial fast drop of the MS signal (lasting ~2 s) that is mainly due to the adsorption process (see Figure 2). Within this time frame, surface coverage is very low, and adsobate−adsorbate interactions are negligible. In parallel, the desorption process starts slowly to compete, leading to saturation within ~100 s. At low $CH_3C(O)OH$ concentrations (<6.5 × 10^{11} molecules cm^{-3}), γ_0 values were independent of $CH_3C(O)OH$ concentration, which verifies that the surface coverage was low during the initial 2 s. However, at $[CH_3C(O)OH] > 6.5 \times 10^{11}$ molecules cm^{-3} and fractional overages $\theta > 0.5$, γ_0 values were decreased with increasing $CH_3C(O)OH$ concentration, like in the HC(O)OH case.[27]

Moreover, the temperature dependence of the initial uptake coefficient, $\gamma_0(T)$, of $CH_3C(O)OH$ on ice films doped with 1.96 and 7.69 wt % HNO_3 was measured at low $CH_3C(O)OH$ concentrations (<6.5 × 10^{11} molecules cm^{-3}) and over the range 198−208 K. The obtained γ_0 values are listed in Table 2, and the Arrhenius plots are shown in Figure 3. It appears that the initial uptake coefficient values of $CH_3C(O)OH$ on pure (A), 1.96 wt % (B), and 7.69 wt % (C) HNO_3-doped ice films were very well-represented by the Arrhenius expressions: $\gamma_{0,A}(T) = (4.73 \pm 1.13) \times 10^{-17} \exp[(6496 \pm 1798)/T]$, $\gamma_{0,B}(T) = (5.88 \pm 0.40) \times 10^{-12} \exp[(4062 \pm 192)/T]$ and $\gamma_{0,C}(T) = (5.66 \pm 0.38) \times 10^{-16} \exp[(5988 \pm 252)/T]$, respectively. The quoted error limits are at 95% level of confidence, and the estimated systematic uncertainty is included in the pre-exponential factor. The inverse temperature dependence of γ_0 indicates that $CH_3C(O)OH$ uptakes on ice surfaces take place via a multistep mechanism involving the formation of an intermediate precursor state. It is worth to note that γ_0 values on pure and HNO_3-doped ice films were equal within experimental error and systematically higher than those of HC(O)OH on pure ice films ($\gamma_0(T) = (3.64 \pm 0.44) \times 10^{-15} \exp[(5378 \pm 668)/T]$),[27] as shown in Figure 3. The large variation in pre-exponential factors reflects the narrow temperature range.

dx.doi.org/10.1021/jp205196t | J. Phys. Chem. A 2012, 116, 2198−2208

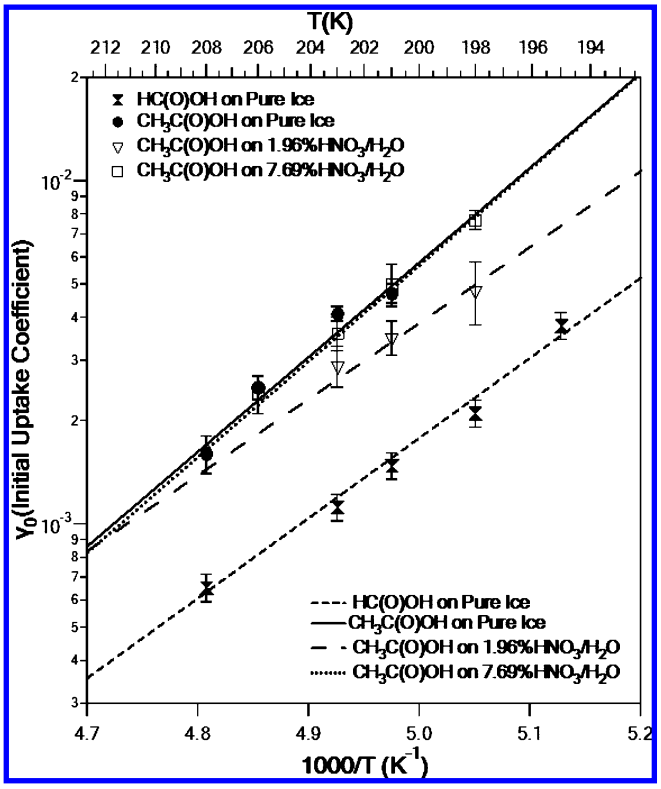

Figure 3. Plot of γ_0 versus $1000/T$ for the adsorption of $CH_3C(O)OH$ on ice films (pure and doped with 1.96 and 7.69 wt % HNO_3) compared to HC(O)OH initial uptake coefficients on pure ice. Error bars reflect the 2σ precision of γ_0 values obtained via eq 2, and in the case of $CH_3C(O)OH$, estimated uncertainties have been added quadratically (see Error Analysis section). Solid, dashed, and dotted lines are the Arrhenius fits of the experimentally determined γ_0 versus $1000/T$ ($\gamma_0 = A\exp(E/RT)$) and along with symbols described as an inset.

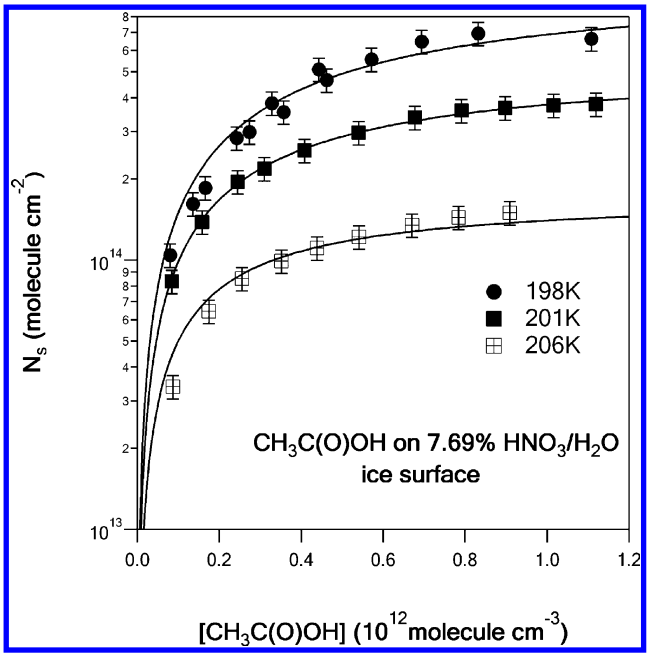

Figure 4. Adsorption isotherms of $CH_3C(O)OH$ on ice films doped with 7.69 wt % HNO_3 at various temperatures. The solid lines are fits of the data according to the Langmuir model in eq 3. Error bars represent the 2σ precision of N_s values.

Surface Coverage of $CH_3C(O)OH$ on Ice. The surface coverage, N_s, of $CH_3C(O)OH$ on pure ice and HNO_3-doped ice films was determined as a function of $CH_3C(O)OH$ concentration in the range $(1.8-11) \times 10^{11}$ molecules cm^{-3} and over the temperatures 198–206 K, and the obtained experimental values are given in Table 3. The adsorption isotherms of $CH_3C(O)OH$ on ice films doped with 7.69 wt % HNO_3 are presented in Figure 4. Each point represents the average value of more than 4 different measurements recorded on fresh ice films to ensure repeatability and reproducibility.

Our experimental data were fitted employing the Langmuir adsorption model that is valid for monolayer adsorptions of gas phase molecules on solid surfaces, and insignificant gas–adsorbate and adsorbate–adsorbate interactions. Both assumptions are generally true at low fractional coverage. In particular, this model is described by the following expression:

$$\theta = \frac{N_s}{N_{max}} = \frac{K_{Lang}[CH_3C(O)OH]}{1 + K_{Lang}[CH_3C(O)OH]} \quad (3)$$

where θ is the fractional coverage of $CH_3C(O)OH$ molecules on the ice surface, N_s is the number of adsorbed $CH_3C(O)OH$ molecules on the ice surface (molecules cm^{-2}), N_{max} is the monolayer saturation surface coverage (molecules cm^{-2}), and K_{Lang} (cm^3 $molecule^{-1}$) is the Langmuir equilibrium constant that describes the partitioning between the gas phase and that adsorbed on the surface molecules. Even for ice films doped with 7.69 wt % HNO_3, in which $CH_3C(O)OH$ uptake signals were leveled-off at later times ($t > 100$ s) reaching at least to 80% of the initial steady-state value ($t = 0$), the Langmuir adsorption model fits our experimental data very well.

Furthermore, eq 3 is rearranged to

$$\frac{[CH_3C(O)OH]}{N_s} = \frac{1}{N_{max}K_{Lang}} + \frac{1}{N_{max}}[CH_3C(O)OH] \quad (4)$$

Therefore, linear least-squares fit of the plots $[CH_3C(O)OH]/N_s$ versus $[CH_3C(O)OH]$ provides N_{max} and K_{Lang} values for the different ice surfaces at various temperatures. These plots are given in Figure 5, along with the linear least-squares fits to eq 4. The obtained N_s values for HNO_3-doped ice films as a function of $CH_3C(O)OH$ concentration at different ice temperatures are given in Table 3. In all cases, the fits of the experimental data were excellent, indicating that the basic assumptions of the Langmuir adsorption model are valid (all adsorption sites of the ice surface are equivalent, and the interactions between adsorbed molecules are negligible). Even for 7.69 wt % HNO_3-doped ice films, where in-bulk diffusion is most likely to occur, the Langmuir adsorption model fits reasonably well with our experimental data. N_{max}, K_{Lang}, and K_{Lin} ($K_{Lin} = N_{max}K_{Lang}$) values, derived from these plots, are presented in Table 4. It should be noticed that N_{max} values for HNO_3-doped ice films, at lower temperatures are higher than those on pure ice, suggesting the appearance of in-bulk diffusion or significant changes in the ice surface morphology and structure. In particular, for 7.69 wt % HNO_3-doped ice films, N_{max} values increase, while K_{Lang} values decrease by decreasing the ice temperature, and such behavior indicates additional processes besides monolayer adsorption. Thus, N_{max}, K_{Lin}, and K_{Lang} values for HNO_3-doped ice films are approximate and are given for comparison reasons.

The plots of eq 4 for pure ice films at different temperatures are shown in Figure 5a and yield the values

dx.doi.org/10.1021/jp205196t | J. Phys. Chem. A 2012, 116, 2198–2208

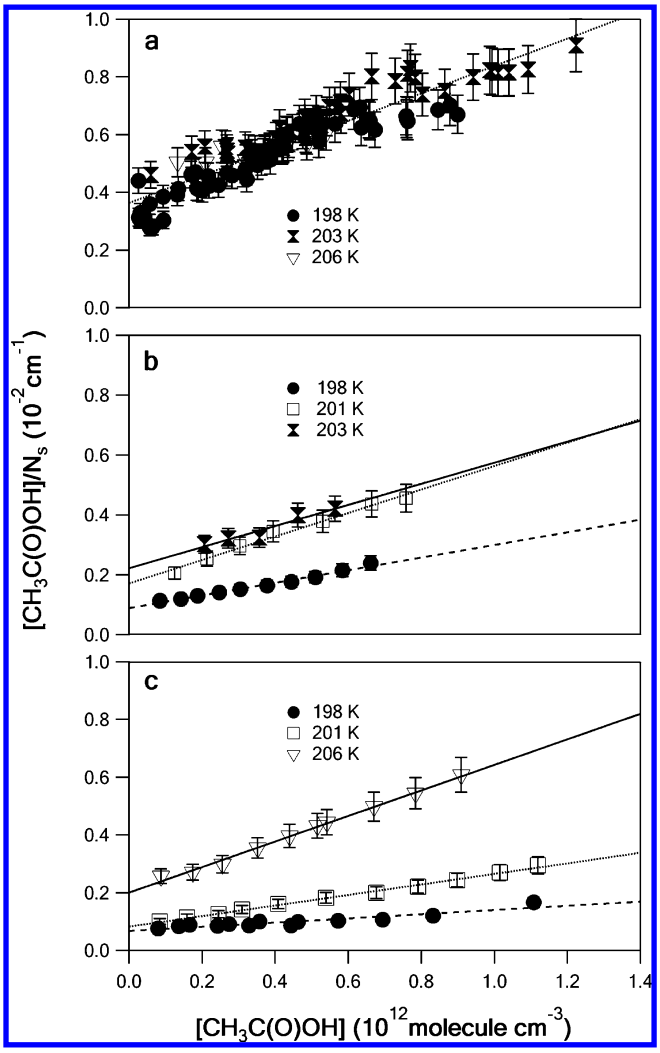

Figure 5. Plots of $[CH_3C(O)OH]/N_s$ versus $[CH_3C(O)OH]$ for $CH_3C(O)OH$ uptakes: (a) on pure ice films, (b) on ice films doped with 1.96 wt % HNO_3, and (c) on ice films doped with 7.69 wt % HNO_3 at several temperatures in the range 198−206 K. The solid lines are fits of the data according to the Langmuir model eq 4. Error bars represent the 2σ precision of N_s values.

N_{max} = (2.11 ± 0.16) × 10^{14} molecules cm^{-2} and K_{Lin} = 274 ± 25 cm. The N_{max} value is in good agreement with the previous experimental values (2−3) × 10^{14}, (2.4 ± 0.6) × 10^{14}, and (2.4 ± 0.2) × 10^{14} molecules cm^{-2} by Sokolov et al.[17] (T = 222−245 K), Hessberg et al.[18] (T = 197 K), and Symington et al.[19] (T = 218 K), respectively. Moreover, our K_{Lin} values are generally lower than those obtained by using the CWLFT technique,[17−20] at higher ice temperatures, and particularly 170 and 50 times lower than those reported by Hessberg et al.[18] at 197 and 209 K, respectively. The cause of this difference remains unclear.

N_{max} values for 1.96 wt % HNO_3-doped ice films, given in Table 4, were (2.54 ± 0.28) × 10^{14} and (4.74 ± 0.43) × 10^{14} molecules cm^{-2} at 201 and 198 K, respectively. It should be noticed that N_{max} values at 201 and 203 K are equal within experimental error, but it doubles at 198 K. In addition, for 7.69 wt % HNO_3-doped ice films (Table 4 and Figure 5c), N_{max} values were decreasing with temperature and were measured to be (1.75 ± 0.10) × 10^{14} and (11.4 ± 1.4) × 10^{14} molecules cm^{-2} at 206 and 198 K, respectively. Similar temperature dependence was observed for K_{Lin} values, as shown in Table 4.

Table 4. Saturation Surface Coverage N_{max} and Partitioning Constants K_{Lang} and K_{Lin} Values for $CH_3C(O)OH$ Uptakes on Pure Ice Films and on Ice Films Doped with 1.96 and 7.69 wt % HNO_3 at Various Temperatures[a]

T (K)	$[CH_3C(O)OH]^b$	$N_{max}{}^c$	$K_{Lang}{}^d$	$K_{Lin}{}^e$
		Pure Ice		
198	0.26−12.4	2.11 ± 0.16	13.0 ± 0.7	274 ± 25
203	0.52−12.2			
206	0.84−5.39			
		Ice Doped with 1.96 wt % HNO_3		
198	0.84−6.61	4.74 ± 0.43	23.4 ± 2.0	1109 ± 138
201	1.25−7.58	2.54 ± 0.28	23.0 ± 4.0	584 ± 120
203	0.78−6.58	2.84 ± 0.94	15.9 ± 5.2	450 ± 209
		Ice Doped with 7.69 wt % HNO_3		
198	0.80−11.1	11.4 ± 1.4	12.8 ± 0.9	1459 ± 206
201	0.84−11.2	5.49 ± 0.24	21.8 ± 1.4	1197 ± 93
206	0.87−9.09	1.75 ± 0.10	22.0 ± 1.5	385 ± 33

[a]The quoted uncertainties are given at 95% level of confidence and correspond to the 2σ precision. [b]$[HC(O)OH]$ in 10^{11} molecules cm^{-3}. [c]N_{max} in 10^{14} molecules cm^{-2}. [d]K_{Lang} in $10^{-13}cm^3$ $molecule^{-1}$. [e]$K_{Lin} = N_{max} \times K_{Lang}$ in cm.

This behavior indicates the presence of in-bulk diffusion and/or morphology changes in HNO_3-doped ice films, which are temperature dependent, and alter the nature of the adsorption uptake interaction. Therefore, it is safe to conclude that the heterogeneous interaction of $CH_3C(O)OH$ with HNO_3-doped ice films are stronger than with pure ice films, leading to higher surface coverage, as shown in Figure 6. Similar behavior

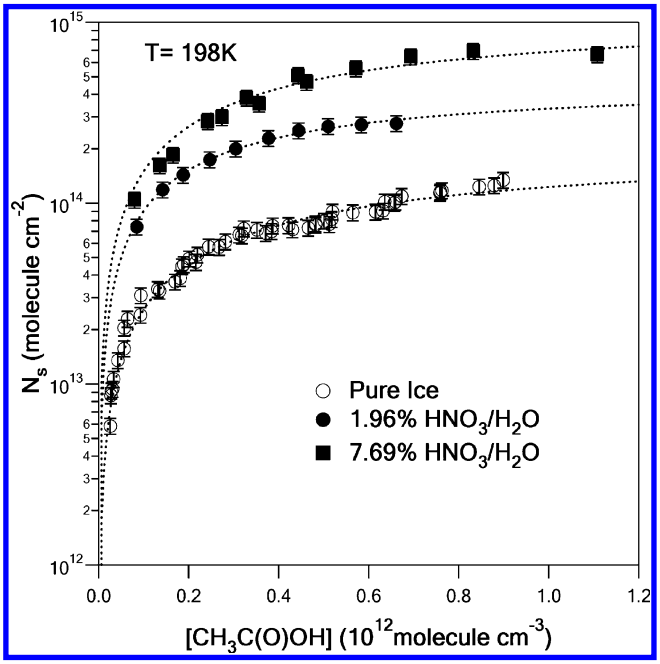

Figure 6. Adsorption isotherms of $CH_3C(O)OH$ on pure ice films and on ice films doped with 1.96 and 7.69 wt % HNO_3 at 198 K. The dotted lines are fits of the data according to the Langmuir model eq 3, and the error bars represent the 2σ precision (10%).

has been observed previously for HC(O)OH.[27] In particular, Figure 6 shows that the uptakes on HNO_3-doped ice films are approximately 3−6 times higher than those on pure ice films, in the whole range of $CH_3C(O)OH$ concentrations. In addition, the uptake signals for $CH_3C(O)OH$ adsorption on pure ice

dx.doi.org/10.1021/jp205196t | J. Phys. Chem. A 2012, 116, 2198−2208

(Figure 2) and 1.96% HNO_3-doped ice films (Supporting Information, Figure S2) were returning to their initial steady-state value within ~100 s. On the contrary, for 7.69% HNO_3-doped ice films (Supporting Information, Figure S2), the uptake signals were saturated at later times reaching ~80% of their initial value at the lowest temperature (198 K).

Atmospheric Implications. The atmospheric lifetime, τ_{het}, of $CH_3C(O)OH$ molecules due to heterogeneous interaction with ice particles in cirrus clouds is given as $1/k_{het}$ by assuming that the ice particles are in equilibrium and are not growing or evaporating. k_{het} is the rate coefficient for the heterogeneous reaction and given by the following expression:

$$k_{het} = \frac{\gamma_0 u A}{4} \quad (5)$$

where γ_0 is the dimensionless initial uptake coefficient, u is the mean molecular velocity (cm s^{-1}), and A is the surface area density (surface to volume ratio, in cm^2 cm^{-3}) of ice ranging between 2×10^{-4} and 2×10^{-7} cm^2 cm^{-3} for cirrus clouds.[39] Therefore, introducing the extreme scenario that all adsorbed molecules are removed from the atmosphere, either via in-cloud processes or precipitation, and that they are not released back to the atmosphere after cirrus cloud evaporation, the atmospheric lifetime (τ_{het}) of $CH_3C(O)OH$ molecules due to the heterogeneous interaction with ice particles in cirrus clouds is given as $1/k_{het}$, (eq 5) at two extreme cloud surface densities. It is worthy to note that this scenario provides an upper limit to the contribution of heterogeneous processes in the removal of $CH_3C(O)OH$ molecules from the atmosphere since a fraction of $CH_3C(O)OH$ molecules will be released back to the atmosphere either during the uptake or after cloud evaporation. However, the formation of new clouds will readsorb a fraction of $CH_3C(O)OH$ molecules and will affect the average steady-state concentration of gaseous $CH_3C(O)OH$. For pure ice surfaces and low A values (2×10^{-7} cm^{-1}), the uptake lifetimes are in the range 44−137 h at the temperature range of 201−208 K. However, since cirrus clouds do not last longer than 24 h, the removal of $CH_3C(O)OH$ molecules by cirrus clouds is negligible. On the other hand, for high A values (2×10^{-4} cm^{-1}) at which uptake lifetimes are much shorter (2−8 min), the heterogeneous removal of $CH_3C(O)OH$ by dense cirrus clouds may not be negligible and should be evaluated as potent sinks of $CH_3C(O)OH$ in that region, in addition to their gas phase photochemistry.

Nevertheless, the heterogeneous uptake of $CH_3C(O)OH$ molecules on dense cirrus clouds in the upper troposphere should be compared with their gas phase reactions with OH radicals and Cl atoms. The lifetimes of $CH_3C(O)OH$ due to the gas-phase reactions are given by the following expression:

$$\frac{1}{\tau} = \frac{1}{\tau_{OH}} + \frac{1}{\tau_{Cl}} = k_{OH}[OH]_{ave} + k_{Cl}[Cl]_{ave} \quad (6)$$

where k_{OH} and k_{Cl} are the rate coefficients of the $CH_3C(O)OH$ reaction with OH radicals and Cl atoms, respectively. The average tropospheric concentrations of OH radicals and Cl atoms, used in eq 6, are $[OH]_{ave} = 8.1 \times 10^5$ cm^{-3},[40] and $[Cl]_{ave} = 1 \times 10^4$ cm^{-3}.[41] The reaction rate coefficients of $CH_3C(O)OH$ with OH radicals[4] and Cl atoms[42,43] are given by the Arrhenius expressions: $(2.2 \pm 0.2) \times 10^{-14}$ $e^{(8.41 \pm 0.67\ kJ/mol)/RT}$ and $(1.00 \pm 0.16) \times 10^{-11}$ $e^{-(14.9 \pm 0.4\ kJ/mol)/RT}$ cm^3 $molecule^{-1}$ s^{-1}, respectively. τ_{OH} and τ_{Cl} values of $CH_3C(O)OH$ within the temperature range 201−208 K are (4−5) days and (1400−2000) years, respectively. Therefore, the heterogeneous uptake of $CH_3C(O)OH$ on dense ice particles, in the upper troposphere, has a stronger contribution in removing acetic acid from this region, compared to the gas phase chemistry, and may locally influence the steady-state concentration of $CH_3C(O)OH$ in UT/LS. Furthermore, the heterogeneous uptakes of $CH_3C(O)OH$ on lightly HNO_3-doped ice particles are higher and almost independent of HNO_3 concentration, as in the $HC(O)OH$ case.[27] However, in order to assess the overall importance of the heterogeneous interaction of $CH_3C(O)OH$ in the atmosphere, one has to consider and model the competition between gas-phase chemistry and heterogeneous processes in the whole range of the atmosphere, by taking into account the dynamic nature and the seasonal dependence of clouds formation, and include in-cloud processes and precipitation effects during a cloud's lifetime.

It should be stressed that eq 5 is not the rate limiting step in the removal of gaseous species from the atmosphere.[24] The fraction, f, of $CH_3C(O)OH$ molecules adsorbed on the ice surface over the gas phase and ice surface, is given by the following expression:

$$f = \frac{CH_3C(O)OH_{ads}}{CH_3C(O)OH_g} = \frac{K_{Lin}A}{1 + K_{Lang}[CH_3C(O)OH]_g} \quad (7)$$

where A is the surface area density (cm^2 cm^{-3}) and K_{Lin} is the partition coefficient between gas-phase molecules and those adsorbed on the ice surface (cm). On the basis of the K_{Lang} determined in the present work and the low gas-phase concentrations of $CH_3C(O)OH$ in the atmosphere ($K_{Lang}[CH_3C(O)OH]_g \ll 1$), the denominator in eq 7 is almost one, and therefore, the ratio of the adsorbed over the total number of $CH_3C(O)OH$ molecules (adsorbed and gas phase molecules) is given by the following expression:

$$a = \frac{CH_3C(O)OH_{ads}}{CH_3C(O)OH_g + CH_3C(O)OH_{ads}} = \frac{K_{Lin}A}{1 + K_{Lin}A} \quad (8)$$

According to eq 8, the removal of $CH_3C(O)OH$ molecules in low and high density cirrus clouds (H_2O) is insignificant (<5%). However, the uptake on binary cirrus cloud particles (HNO_3/H_2O) needs further evaluation since the fraction of the adsorbed gas phase $CH_3C(O)OH$ molecules becomes substantially higher, reaching up to 20% for mixing ratios of 7.69 wt % HNO_3/H_2O.

■ CONCLUSIONS

The heterogeneous interaction of $CH_3C(O)OH$ with thin ice or HNO_3-doped ice films was studied at various $CH_3C(O)OH$ concentrations and low temperatures, relevant to the UT/LS. The initial uptake coefficients, γ_0, of $CH_3C(O)OH$ on ice surfaces were measured for the first time and determined to be in the range $(1.6–7.7) \times 10^{-3}$. The temperature dependence of γ_0 for $CH_3C(O)OH$ molecules on thin ice films is given by the Arrhenius expression $\gamma_0(T) = (4.73 \pm 1.13) \times 10^{-17} \exp[(6496 \pm 1798)/T]$, exhibiting inverse to temperature dependence suggesting a multistep uptake mechanism and the existence of an intermediate precursor state. There was no evidence of in-bulk diffusion, dissociation, nor ionization of $CH_3C(O)OH$ on the pure ice surfaces. Uptake signals on pure and 1.96% HNO_3-doped ice surfaces were returning to their initial steady-state value within ~100 s, and the surface coverages, N_s, were well

represented by the Langmuir adsorption model. Saturation surface coverage, N_{max}, of $CH_3C(O)OH$ on thin ice films was measured to be $(2.11 \pm 0.16) \times 10^{14}$ molecules cm^{-2}, in excellent agreement with the literature. Furthermore, N_{max} values of $CH_3C(O)OH$ on HNO_3-doped ice films (1.96 and 7.69 wt %) were larger compared to those on pure ice films and were exhibiting inverse temperature dependence. Such behavior is attributed to stronger gas−ice surface interactions and/or in-bulk diffusion leading to more efficient uptakes. The atmospheric lifetime, τ_{het}, of $CH_3C(O)OH$ molecules due to heterogeneous interaction with ice particles in dense cirrus clouds at UT/LS temperatures was estimated to be in the range 2−8 min, which is much shorter than the lifetime (4−5 days) due to gas-phase chemistry (OH and Cl initiated reactions). Finally, $CH_3C(O)OH$ molecules may be partially and locally removed by uptake on dense cirrus clouds in the UT/LS, in regions containing HNO_3-doped ice particles.

■ ASSOCIATED CONTENT

Supporting Information

Typical MS signal−flow calibration plots of mass spectral intensity (I_M) versus molecular flow rate (F_M) for H_2O and $CH_3C(O)OH$. Typical profiles of uptake signals for $CH_3C(O)OH$ on 1.96 and 7.69 wt % HNO_3-doped ice films. Typical calibration plot of MS signal intensity $I_{CH3C(O)OH}$ versus molecular flow rate $F_{CH3C(O)OH}$. This material is available free of charge via the Internet at http://pubs.acs.org.

■ AUTHOR INFORMATION

Corresponding Author

*Tel: +302810545031. Fax: +302810545001. E-mail: panosp@chemistry.uoc.gr.

Notes

The authors declare no competing financial interest.

■ ACKNOWLEDGMENTS

This article is dedicated to the memory of Professor Sidney W. Benson, among the founders of chemical kinetics and thermochemistry, and above all, a brilliant scientist and magnificent person who inspired and shaped the scientific career of many chemists of our generation. This work was financially supported by a research grant from the Hellenic Ministry of Education under the program "PENED 2003" and the European Union by the project SCOUT-O_3, EVK2-CT-1999-00005. This study was carried out in partial fulfillment of a doctoral and master dissertation (to M.N.R. and A.G.Z.) at the Chemistry Department, University of Crete, Greece.

■ REFERENCES

(1) Khare, P.; Kumar, N.; Kumari, K. M.; Srivastava, S. S. *Rev. Geophys.* **1999**, *37*, 227−248.
(2) Rinsland, C. P.; Mahieu, E.; Zander, R.; Goldman, A.; Wood, S.; Chiou, L. *J. Geophys. Res., [Atmos.]* **2004**, *109*, D18308−D18315.
(3) Legrand, M.; Preunkert, S.; Jourdain, B.; Aumont, B. *J. Geophys. Res., [Atmos.]* **2004**, *109*, D06313−D06323.
(4) Butkovskaya, N. I.; Kukui, A.; Pouvesle, N.; Le Bras, G. *J. Phys. Chem. A* **2004**, *108*, 7021−7026.
(5) Paulot, F.; Wunch, D.; Crounse, J. D.; Toon, G. C.; Millet, D. B.; DeCarlo, P. F.; Vigouroux, C.; Deutscher, N. M.; González Abad, G.; Notholt, J.; et al. *Atmos. Chem. Phys.* **2011**, *11*, 1989−2013.
(6) Chameides, W. L.; Davis, D. D. *Nature* **1983**, *304*, 427−429.
(7) Gayet, J. F.; Febvre, G.; Brogniez, G.; Chepfer, H.; Renger, W.; Wendling, P. *J. Atmos. Sci.* **1996**, *53*, 126−138.
(8) Singh, H.; Chen, Y.; Tabazadeh, A.; Fukui, Y.; Bey, I.; Yantosca, R.; Jacob, D.; Arnold, F.; Wohlfrom, K.; Atlas, E.; et al. *J. Geophys. Res., [Atmos.]* **2000**, *105*, 37795−33805.
(9) Laaksonen, A.; Hienola, J.; Kulmala, M.; Arnold, F. *Geophys. Res. Lett.* **1997**, *24*, 3009−3012.
(10) Fahey, D. W.; Gao, R. S.; Carslaw, K. S.; Kettleborough, J.; Popp, P. J.; Northway, M. J.; Holecek, J. C.; Ciciora, S. C.; McLaughlin, R. J.; Thompson, T. L.; et al. *Science* **2001**, *291*, 1026−1031.
(11) Popp, P. J.; Gao, R. S.; Marcy, T. P.; Fahey, D. W.; Hudson, P. K.; Thompson, T. L.; Karcher, B.; Ridley, B. A.; Weinheimer, A. J.; Knapp, D. J.; et al. *J. Geophys. Res., [Atmos.]* **2004**, *109*, D06302−D06315.
(12) Hudson, P. K.; Zondlo, M. A.; Tolbert, M. A. *J. Phys. Chem. A* **2002**, *106*, 2882−2888.
(13) Dominé, F.; Rey-Hanot, L. *Geophys. Res. Lett.* **2002**, *29*, 1873−1876.
(14) Winkler, A. K.; Holmes, N. S.; Crowley, J. N. *Phys. Chem. Chem. Phys.* **2002**, *2*, 5270−5275.
(15) Abbatt, J. P. D. *Chem. Rev.* **2003**, *103*, 4783−4800.
(16) Peybernès, N.; Marchand, C.; Le Calvé, S.; Mirabel, P. *Phys. Chem. Chem. Phys.* **2004**, *6*, 1277−1284.
(17) Sokolov, O.; Abbatt, J. P. D. *J. Phys. Chem.* **2002**, *106*, 775−782.
(18) Hessberg, P. V.; Pouvesle, N.; Winkler, A. K.; Schuster, G.; Crowley, J. N. *Phys. Chem. Chem. Phys.* **2008**, *10*, 2345−2355.
(19) Symington, A.; Cox, R. A.; Fernandez, M. A. *Z. Phys. Chem.* **2010**, *224*, 1219−1245.
(20) Kerbrat, M.; Huthwelker, T.; Bartels-Rausch, T.; Gaggeler, H. W.; Ammann, M. *Phys. Chem. Chem. Phys.* **2010**, *12*, 7194−7202.
(21) Compoint, M.; Toubin, C.; Picaud, S.; Hoang, P. N. M.; Girardet, C. *Chem. Phys. Lett.* **2002**, *365*, 1−7.
(22) Picaud, S.; Hoang, P. N. M.; Peybernès, N.; Le Calve, S.; Mirabel, P. *J. Chem. Phys.* **2005**, *122*, 194707−194716.
(23) Allouche, A.; Bahr, S. *J. Phys. Chem. B* **2006**, *110*, 8640−8648.
(24) Crowley, J. N.; Ammann, M.; Cox, R. A.; Hynes, R. G.; Jenkin, M. E.; Mellouki, A.; Rossi, M. J.; Troe, J.; Wallington, T. J. *Atmos. Chem. Phys.* **2010**, *10*, 9059−9223.
(25) Kambanis, K. G.; Lazarou, Y. G.; Papagiannakopoulos, P. *J. Chem. Soc. Faraday Trans.* **1996**, *92*, 3299−3303.
(26) Papadimitriou, V. C.; Papanastasiou, D. K.; Stefanopoulos, V. G.; Zaras, A. M.; Lazarou, Y. G.; Papagiannakopoulos, P. *J. Phys. Chem. A* **2007**, *111*, 11608−11617.
(27) Romanias, M. N.; Zogka, A. G.; Stefanopoulos, V. G.; Papadimitriou, V. C.; Papagiannakopoulos, P. *ChemPhysChem* **2010**, *11*, 4042−4052.
(28) Pratte, P.; Bergh, H. V. D.; Rossi, M. J. *J. Phys. Chem. A* **2006**, *110*, 3042−3058.
(29) Beyer, K. D.; Hansen, A. R. *J. Phys. Chem. A* **2002**, *106*, 10275−10284.
(30) Boxe, C. S.; Bodsgard, B. R.; Smythe, W.; Leu, M. T. *J. Colloid Interface Sci.* **2007**, *309*, 412−418.
(31) Kayser, L. F.; Leu, M. T. *Microsc. Res. Tech.* **1993**, *25*, 434−438.
(32) Kayser, L. F.; Leu, M. T. *J. Colloid Interface Sci.* **1993**, *155*, 137−145.
(33) Delval, C.; Rossi, M. J. *J. Phys. Chem. A* **2005**, *109*, 7151−7165.
(34) Worsnop, D. R.; Fox, L. E.; Zahniser, M. S.; Wofsy, S. C. *Science* **1993**, *259*, 71−74.
(35) Chao, J.; Zwolinski, B. J. *J. Phys. Chem. Ref. Data* **1978**, *7*, 363−377.
(36) Büttner, R.; Maurer, G. *Ber. Bunsenges. Phys. Chem.* **1983**, *87*, 877−882.
(37) Hellebust, S.; O'Riordan, B.; Sodeau, J. *J. Chem. Phys.* **2007**, *126*, 084702−084713.
(38) Huthwelker, T.; Ammann, M.; Thomas, T. *Chem. Rev.* **2006**, *106*, 1375−1444.
(39) Solomon, S.; Borrmann, S.; Garcia, R. R.; Portmann, R.; Thomason, L.; Poole, L. R.; Winker, D.; McCormick, M. P. *J. Geophys. Res.* **1997**, *102*, 21411−21429.

(40) Prinn, R. G.; Huang, J.; Weiss, R. F.; Cunnold, D. M.; Fraser, P. J.; Simmonds, P. G.; McCulloch, A.; Harth, C.; Salameh, P.; O'Doherty, S.; et al. *Science* **2001**, *292*, 1882−1888.
(41) Wingenter, O. W.; Sive, B. C.; Blake, N. J.; Blake, D. R.; Rowland, F. S. *J. Geophys. Res.* **2005**, *110*, D20308−D20317.
(42) Atkinson, R.; Baulch, D. L.; Cox, R. A.; Crowley, J. N.; Hampson, R. F.; Hynes, R. G.; Jenkin, M. E.; Rossi, M. J.; Troe, J.; Wallington, T. J. *Atmos. Chem. Phys.* **2008**, *8*, 4141−4496.
(43) Romanias, M.; Lazos, E.; Stefanopoulos, V. G.; Papadimitriou, V. C.; Papagiannakopoulos, P. 2012, to be published.